ACCOUNTS of chemical research

Article

pubs.acs.org/accounts

Dielectric Force Microscopy: Imaging Charge Carriers in Nanomaterials without Electrical Contacts

Jie Zhang,[∥] Wei Lu, Yize Stephanie Li,[⊥] Jinhua Cai, and Liwei Chen*

i-Lab, Suzhou Institute of Nano-Tech and Nano-Bionics, Chinese Academy of Sciences, Suzhou, Jiangsu 215123, China

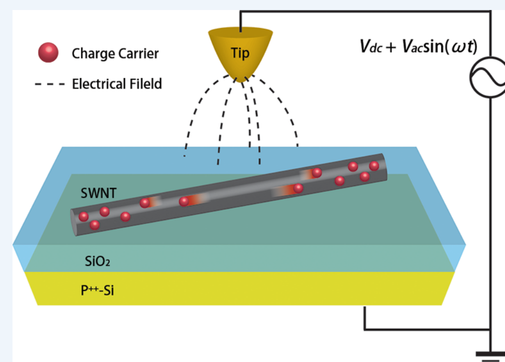

CONSPECTUS: Nanomaterials are increasingly used in electronic, optoelectronic, bioelectronic, sensing, and energy nanodevices. Characterization of electrical properties at nanometer scales thus becomes not only a pursuit in basic science but also of widespread practical need. The conventional field-effect transistor (FET) approach involves making electrical contacts to individual nanomaterials. This approach faces serious challenges in routine characterization due to the small size and the intrinsic heterogeneity of nanomaterials, as well as the difficulties in forming Ohmic contact with nanomaterials. Since the charge carrier polarization in semiconducting and metallic materials dominates their dielectric response to external fields, detecting dielectric polarization is an alternative approach in probing the carrier properties and electrical conductivity in nanomaterials. This Account reviews the challenges in the electrical conductivity characterization of nanomaterials and demonstrates that dielectric force microscopy (DFM) is a powerful tool to address the challenges. DFM measures the dielectric polarization via its force interaction with charges on the DFM tip and thus eliminates the need to make electrical contacts with nanomaterials. Furthermore, DFM imaging provides nanometer-scaled spatial resolution.

Single-walled carbon nanotubes (SWNTs) and ZnO nanowires are used as model systems. The transverse dielectric permittivity of SWNTs is quantitatively measured to be ∼10, and the differences in longitudinal dielectric polarization are exploited to distinguish metallic SWNTs from semiconducting SWNTs. By application of a gate voltage at the DFM tip, the local carrier concentration underneath the tip can be accumulated or depleted, depending on charge carrier type and the density of states near the Fermi level. This effect is exploited to identify the conductivity type and carrier type in nanomaterials.

By making comparison between DFM and FET measurements on the exact same SWNTs, it is found that the DFM gate modulation ratio, which is the ratio of DFM signal strengths at different gate voltage, is linearly proportional to the logarithm of FET device on/off ratio. A Drude-level model is established to explain the semilogarithmic correlation between DFM gate modulation ration and FET device on/off ratio and simulate the dependence of DFM force on charge carrier concentration and mobility. Future developments towards DFM imaging of charge carrier concentration or mobility in nanomaterials and nanodevices can thus be expected.

■ INTRODUCTION

Electricity and magnetism-based technologies have become a signature of the modern civilization. In recent decades, characterization of unique electrical conduction behavior at the nanometer scale and the exploration of its applications in electronic devices constitute a major driving force behind the explosive development of nanoscience and nanotechnology.[1−4] As more and more nanomaterials seek their applications in electronic, optoelectronic, bioelectronic, sensing, and energy nanodevices, characterization of electrical properties at nanometer scales is not only a pursuit in basic science but also of widespread practical need.

The mainstream approach of measuring electrical conductivity of nanomaterials involves making metal contacts to the specific piece of nanomaterial of interest and then measuring electrical transport through the structure using sourcemeters.[5] Extra front or back gate electrodes or both can be applied to control the charge carriers in the material, effectively forming a field-effect transistor (FET), which allows for probing of electrical conductivity and charge carrier behavior within a much broader parameter window.[6−8] This approach has gained great success in various fields ranging from materials science and condensed matter physics to electrical engineering.[9−11] However, as widespread applications seek routine characterization of large amounts of heterogeneous nanomaterials, the limitations of this approach start to emerge. First of all, making electrical contacts to nanometer-sized materials requires special facilities and processing. Since the formation of Ohmic contacts is not always trivial, the deconvolution of the influence of contacts from the intrinsic property of the materials may become a challenge. On the other hand, nanomaterials are intrinsically heterogeneous and thus comprehensive characterization of a sample requires the electrical measurement over a large ensemble of individual

Received: January 29, 2015
Published: June 10, 2015

 © 2015 American Chemical Society

DOI: 10.1021/acs.accounts.5b00046
Acc. Chem. Res. 2015, 48, 1788−1796

nanomaterials in order for the statistics to be meaningful and reliable.

An alternative approach has been developed in the semiconductor industry to characterize the conductivity of materials via their dielectric response to external fields.[12] The dielectric response of semiconductor and metal is dominated by polarization due to mobile carrier motion. Since both electrical conductivity and dielectric response are determined by charge carrier concentration and mobility, the dielectric response of a material indirectly reflects its electrical conductivity. In bulk materials, capacitance−voltage measurement is a standard test to monitor the doping concentration and carrier mobility of silicon materials.[12,13] Scanning probe techniques, such as scanning capacitance microscopy, scanning microwave microscopy, and scanning microwave impedance microscopy, have been developed to image local transport behavior.[14,15]

The challenge of applying the dielectric measurement to nanomaterials is that the dielectric response is an extensive quantity, that is, the induced dipole moment under an external field is proportional to the total mass or volume of the material. In the nanomaterials case, the size in one or more dimensions is limited to less than 100 nm; therefore, the dielectric polarization could be too small for traditional capacitance measurements. Scanning force microscopy (SFM) based techniques thus have taken advantage of the extremely high force sensitivity (approximately piconewton) to measure the dielectric response and carrier dynamics in nanomaterials.[16−18] In particular, dielectric force microscopy (DFM) has demonstrated sensitive detection of the dielectric response and hence the electric conductivity of nanomaterials, with added benefits of spatial resolution and metal contact-free measurement setup.[19] In this Account, we review the principle of the DFM technique and the application of DFM enabled by its unique capabilities and also provide an outlook of this technique.

■ PRINCIPLE OF DFM

The DFM technique was originally developed as the 2ω channel of electrostatic force microscopy (EFM).[21,22] In a double-pass imaging process, the standard AC mode is employed in the first scan to acquire the topographic profile of the sample; the tip is then lifted up by a certain height and an external bias voltage is applied between the conducting tip and the substrate in the second scan (Figure 1a).[19,20] The total force on the tip in the second scan, F, is the sum of two components: Coulombic force, F_{cou}, due to the static charge and multipoles of the sample and capacitance force, F_{cap}, due to surface potential and dielectric response:[22]

$$F = F_{\mathrm{cou}} + F_{\mathrm{cap}} = E_z Q_{\mathrm{tip}} + \frac{1}{2}\frac{\mathrm{d}C}{\mathrm{d}z}V^2 \qquad (1)$$

where E_z is the z-component of the electrical field produced by the static charge and multipole moments on the surface, Q_{tip} is the charge on the tip, C is the capacitance between tip and substrate, z is the separation between the tip and substrate, and $V = V_{dc} + \varphi + V_{ac}\sin(\omega t)$ is the bias voltage applied to the tip, in which V_{dc} is a DC bias voltage, V_{ac} is the amplitude of an AC bias component, and φ is the contact potential difference (CPD) between the tip and sample.

Detailed expansion of eq 1 reveals components of force, F, with different AC frequency characteristics.[20,22,23] Since the charge on the tip is proportional to $\sin(\omega t)$, the Coulombic force between the tip charge and the static charge or multipole

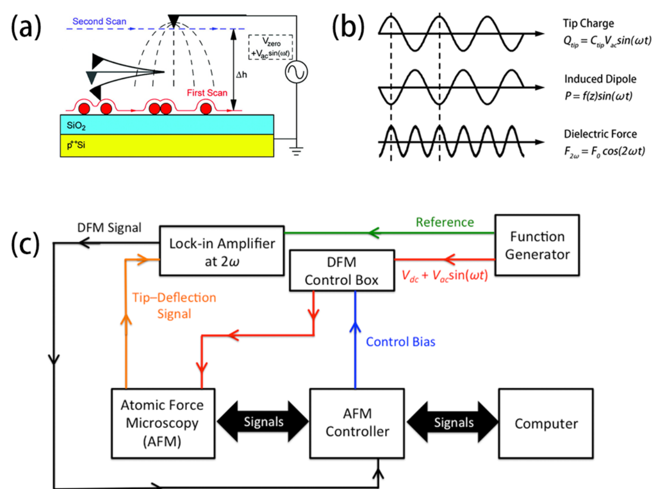

Figure 1. (a) Schematic illustration of the double-passed scan operation of DFM. Reproduced from ref 19. Copyright 2012 American Chemical Society. (b) The interaction between the charge on tip and the induced dipole on sample. Adapted from ref 20. (c) Block diagram of DFM experimental setup, in which the DFM control box only transmits the signal during the second scan.

moments at the sample surface is also proportional to $\sin(\omega t)$ and thus oscillates at the ω frequency. This data channel represents the electrostatic interaction and is the focus of typical EFM measurements.[22] On the other hand, the dielectric polarization of the sample resulting from the external AC bias is also proportional to $\sin(\omega t)$; the dielectric interaction between the induced dipole moment and the tip charge becomes proportional to $\sin^2(\omega t)$, which equals $1/2 - 1/2\cos(2\omega t)$ and thus oscillates at the 2ω frequency (Figure 1b).[20] This channel of data represents the dielectric response of the sample and thus is dubbed as DFM. The block diagram of the DFM experimental setup is laid out in Figure 1c. Typically, the AC angular frequency ω is set around 10 kHz, far below the resonance frequency of the cantilever. Lock-in amplifiers are employed to demodulate the ω and 2ω components from the tip deflection signal, and the ω and 2ω components are then fed back to the AFM controller to generate EFM and DFM images, respectively.

The DFM signal, that is, the dielectric interaction force, can be quantitatively determined provided that the spring constant of the DFM cantilever is calibrated. The quantitative results can be compared with numerical simulations of the DFM signal strength using various models, such as macroscopic continuum models,[20] in which dielectric constants are the parameters reflecting the dielectric properties, and microscopic Drude-level models with carrier concentration and mobility as adjustable parameters.[24]

■ DIELECTRIC PERMITTIVITY OF NANOMATERIALS

The DFM setup enables many interesting measurements. For example, the dielectric permittivity of single-walled carbon nanotubes (SWNTs) can be individually measured.[20] As-synthesized SWNTs are usually a mixture of individual SWNTs with different diameter and chirality, which are manifested in electrical conductivity as a mixture of metallic and semiconducting nanotubes. The dielectric property of SWNTs is expected to be dependent on their diameter and chirality[25−28] and thus can be exploited for the separation of SWNTs in methods such as dielectrophoresis.[29−31] However, the dielectric

DOI: 10.1021/acs.accounts.5b00046
Acc. Chem. Res. 2015, 48, 1788−1796

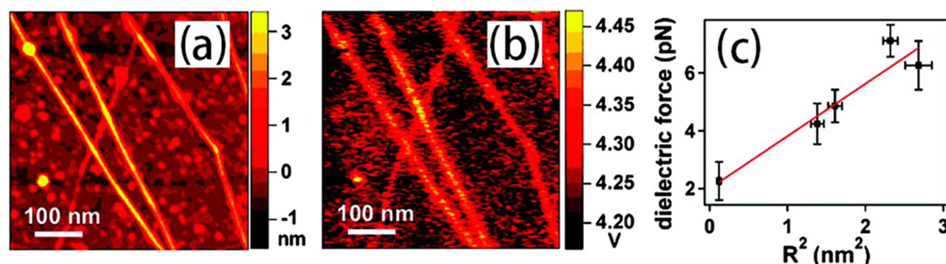

Figure 2. Topographical (a) and dielectric response (b) images of SWNTs and (c) quadratic dependence of the dielectric responses on SWNT radius. Reproduced from ref 20. Copyright 2007 American Chemical Society.

response of individual SWNTs has been rarely investigated experimentally. The scanning proximal probe nature renders the DFM technique essentially a single-molecule approach to overcome the heterogeneity challenge in SWNT ensemble samples.

Chemical vapor deposition (CVD) grown SWNTs are imaged with DFM.[20] Figure 2a,b shows typical topographical and dielectric images. Figure 2c indicates that the dielectric polarization signal intensity is quadratically dependent on the tube radius, suggesting that the near-DC transverse polarizability, $\alpha_\perp$, of carbon nanotubes can be approximated by a solid cylinder with radius R and isotropic dielectric constant ε: $\alpha_\perp = {}^1/_2[(\varepsilon - 1)/(\varepsilon + 1)]R^2$.

Quantification of the SWNT dielectric permittivity requires numerical modeling and thorough understanding of the tip–substrate capacitance, which can be calibrated using a sphere/cone/parallel-plate model.[22] A three-dimensional model can be built around the SWNT and the DFM tip according to the experimental setup, and a finite element analysis package (Multiphysics 3.3, COMSOL, Inc., Burlington, MA) is used to solve the Poisson's equation. The interaction between tip and SWNT is then calculated as $F = \oint_{\text{tip}-\text{surface}} {}^1/_2\vec{D}\cdot\vec{E}\cdot ds$, where $\vec{E}$ is the electric field and $\vec{D} = \varepsilon\varepsilon_0\vec{E}$ is the electric displacement. The dielectric characteristics of the SWNT are tried, and the resulting interaction force is compared with experiments. A typical cross section view of the solved electrical potential distribution is displayed in Figure 3a.

SWNTs are highly anisotropic materials. While their transverse dielectric constants are independent of the structure, the longitudinal dielectric properties are highly sensitive to the chirality and able to differentiate between metallic and semiconducting tubes.[25,28] The influence of longitudinal polarization is observed in both experiments and modeling. Anisotropic semiconducting models with longitudinal permittivity, $\varepsilon_\parallel$, set to 30 (Figure 3b) and metallic models with $\varepsilon_\parallel$ set to 1000 (Figure 3c) along with trials of different transverse permittivity, $\varepsilon_\perp$, are compared against experimental data points. The results show that most tubes are well fit with the semiconducting model ($\varepsilon_\parallel$ = 30, $\varepsilon_\perp$= 10), except for one particular tube (indicated with the black arrow), which requires the metallic model ($\varepsilon_\parallel$ = 1000, $\varepsilon_\perp$= 10) for a good fit. An $\varepsilon_\perp$ of 10, irrespective of metallic or semiconducting tubes, leads to a coefficient C of ~0.41 in the transverse polarizability: $\alpha_\perp = {}^1/_2[(\varepsilon_\perp - 1)/(\varepsilon_\perp + 1)]R^2 = CR^2$, which is consistent with the theoretical predication of C = 0.40 and also verified by Cui et.al. using optical measurements.[28,32] This work is the first experimental measurement of the near-dc polarization of individual SWNTs. Recently, similar setup has been utilized to measure the dielectric permittivity of thin films, dielectric particles, and viruses,[33−37] indicating potentially widespread applications of the DFM technique in nanomaterial characterization.

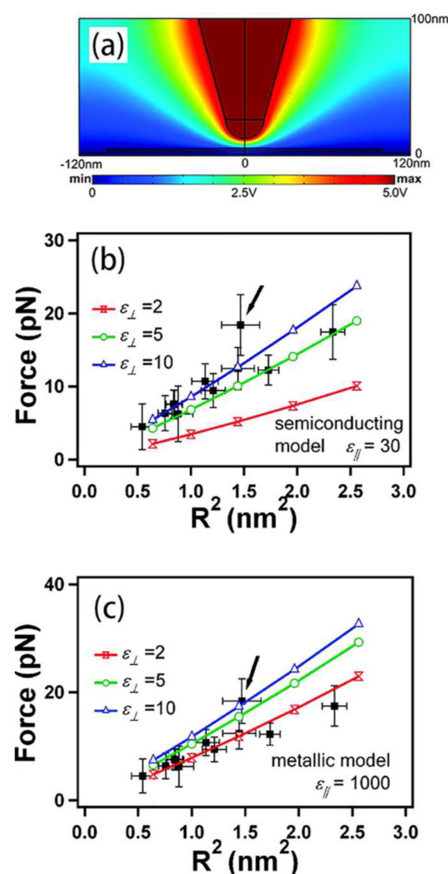

Figure 3. (a) The cross-section view of numerically solved electrical potential distribution at the vicinity of the tip and SWNT. Experimental dielectric response of SWNTs fitted by anisotropic (b) semiconducting and (c) metallic models. Reproduced from ref 20. Copyright 2007 American Chemical Society.

The differentiation between metallic and semiconducting SWNTs in DFM measurements can be further optimized and exploited as an assay for the metallic/semiconducting content in SWNT samples.[23] By the choice of a Si wafer substrate with 50 nm thermal oxide, the DFM contrast between metallic and semiconducting SWNTs is maximized. In a typical experiment, DFM signals of 72 individually dispersed SWNTs were averaged along their length and plotted against their average diameter squared (Figure 4). Two distinctive zones are observed with a separating gap between them. Based on the numerical simulation, the data points in the top and bottom zones are metallic and semiconducting tubes, respectively. This

DOI: 10.1021/acs.accounts.5b00046
Acc. Chem. Res. 2015, 48, 1788−1796

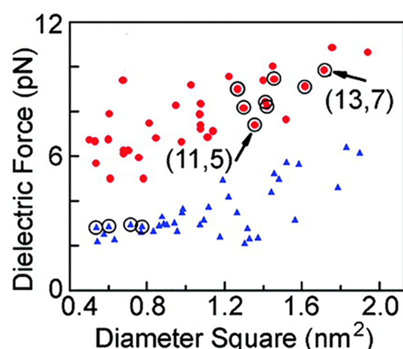

Figure 4. Dielectric responses of SWNTs are plotted as a function of diameter squared. Circled data points correspond to SWNTs that give identifiable signals in confocal Raman imaging. Reproduced from ref 23. Copyright 2009 American Chemical Society.

assignment is confirmed with confocal Raman imaging and resonance Raman spectroscopy.[23] This method was further corroborated with metallic and semiconducting tube enriched samples obtained with DNA wrapping and ion exchange chromatography.[23] The metallic tube content in commericial CoMoCAT and HiPCo SWNTs samples were determined to be 14% and 28%, respectively.

IMAGING CHARGE CARRIERS IN NANOMATERIALS

The dielectric permittivity of metallic and semiconducting nanomaterials is dominated by mobile charge carriers. Measurements on SWNTs and ZnO nanowires demonstrate that the DFM technique is capable of imaging charge carriers in nanomaterials.[19] The basic idea is very similar to the tuning of carrier concentration with a gate voltage in FET. As illustrated in Figure 5a, a gate DC voltage, V_g, is applied to the DFM tip along with the AC probing voltage in the second scan, thus the total voltage on the tip is $V_{total} = V_{zero} + V_g + V_{ac} \sin(\omega t)$, in which V_{zero} is a DC voltage compensating the surface potential difference between the tip and the sample. Depending on the carrier type in the sample and the polarity of V_g at the tip, the gate voltage can cause local accumulation or depletion of charge carriers underneath the tip (Figure 5b) and thus greatly affect the DFM signal strength.

Figure 5c−n exhibits three types of gating behavior, representing metallic, p-type semiconducting, and n-type semiconducting nanomaterials, respectively. The charge carrier concentration can hardly be affected in metallic SWNTs,[38] and thus the DFM signal strength is nearly unaltered under −2, 0, and 2 V gate voltages (Figure 5d−f). In semiconducting SWNTs, the DFM signal is strong under −2 V gate and decreases at 0 and 2 V gate (Figure 5h−j), indicating p-type semiconducting behavior where holes are the majority carriers. Semiconducting SWNTs are indeed known to exhibit p-type doping due to defects or oxygen adsorption.[39,40] On the other hand, the ZnO nanowire displays n-type behavior, that is, stronger signal under 2 V gate and weaker under 0 V and −2 V gate voltages (Figure 5l−n), which is consistent with the expectation that ZnO nanowires are usually n-doped.[41] These experiments indicate that the DFM technique is generally applicable to various nanomaterials and it is capable of identifying the conductivity type, that is, metallic or semiconducting, and in the latter case, identifying the majority charge carrier type.

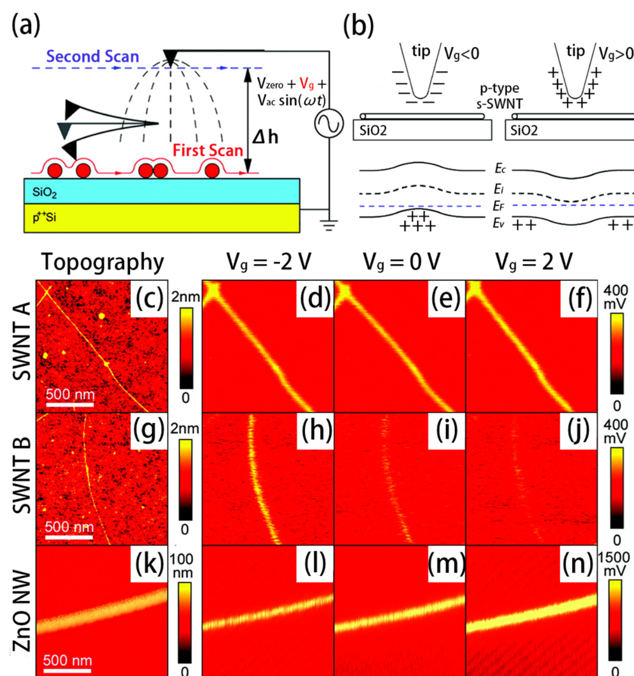

Figure 5. Schematic illustration of (a) the DC gate voltage on tip and (b) carrier distribution in a semiconducting SWNT under different tip gate voltage. E_c and E_v are the conduction and valence band edge, respectively. E_F and E_i denote the Fermi level and the midgap energy level, respectively. (c−n) Topographical and dielectric response images of metallic and semiconducting SWNTs, and a ZnO nanowire. Reproduced from ref 19. Copyright 2012 American Chemical Society.

SPATIAL MAPPING AND *IN SITU* MEASUREMENT CAPABILITY

As a contactless local imaging technique, DFM apparently inherits its spatial mapping capability from being a member of the SFM family. Figure 6 demonstrates this feature using SWNTs as a model system. Figure 6a shows an individual SWNT with regular morphology, but the dielectric response channel indicates the presence of a metal−semiconducting (M−S) intratube junction (Figure 6b−d). Another example in Figure 6e−h shows a SWNT with two M−S intratube junctions. Similar M−S intratube junctions are widely observed in commercial HiPCo, CoMoCAT tubes, or homegrown CVD SWNTs. The location of such junctions will be unidentifiable

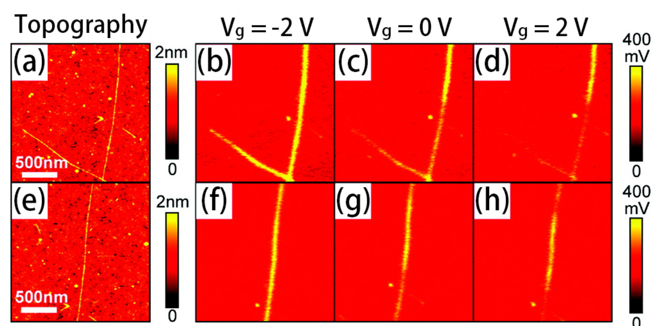

Figure 6. Topographical (a) and dielectric response (b−d) images of a SWNT with an M−S intratube junction. The topographical (e) and dielectric response (f−h) images of a SWNT with an S−M−S intratube junction. Reproduced from ref 19. Copyright 2012 American Chemical Society.

DOI: 10.1021/acs.accounts.5b00046
Acc. Chem. Res. 2015, 48, 1788−1796

using FET charge transport measurement and will be difficult to map with micro-Raman imaging because of the optical resonance requirement as well as the relatively low spatial resolution (∼1 μm).

Another advantage of DFM is its potential in *in situ* measurements due to versatile imaging environments of SFM. This feature is demonstrated in the following investigation on the electronic doping of SWNTs by gaseous ammonia.[42] The interaction between nanomaterials and the gaseous environment is very important in understanding the mechanism of gas-sensing devices, as well as in improving the stability of individual nanomaterial based FET devices. In the cases of SWNT based FET and sensing devices, the Schottky barrier at the SWNT/metal contact often dominates the transport behavior.[43] Contactless DFM measurements are thus ideally suited for probing the intrinsic interactions between nanomaterials and the gaseous environment, in this case, between SWNTs and NH_3.

As shown in Figure 7a, SWNT sample dispersed on Si substrate with 50 nm thermal oxide is first imaged in an enclosed gas chamber filled with nitrogen. The gas environment is then changed to contain increasing amounts of NH_3 and eventually purged back to N_2. The matrix of images in Figure 7b shows the dielectric responses of one particular SWNT in different gas environment and at different tip gating voltage. Images in row A were obtained in pure N_2, revealing a M−S intratube junction with the left portion of the tube being metallic, and the right portion of the tube being p-type semiconducting. In rows B, C, D, and E, the NH_3 content is increased to 5%, 50%, and 100%, and then purged back to 0%, respectively. The images show that the metallic SWNT remains stable at both gate voltage and NH_3 concentration changes. On the other hand, the semiconducting section of the tube displays different behavior. Upon exposure to 5% ammonia (row B), the DFM signal becomes indistinguishable from the background, suggesting nearly depleted hole concentration, and further increase of ammonia concentration to 50% and 100% (rows C and D) brings back the DFM signal, but intriguingly, the DFM signal now increases with increasing gate voltage, indicating that charge carrier type in this SWNT has been inverted to electrons under high concentration of gaseous ammonia.

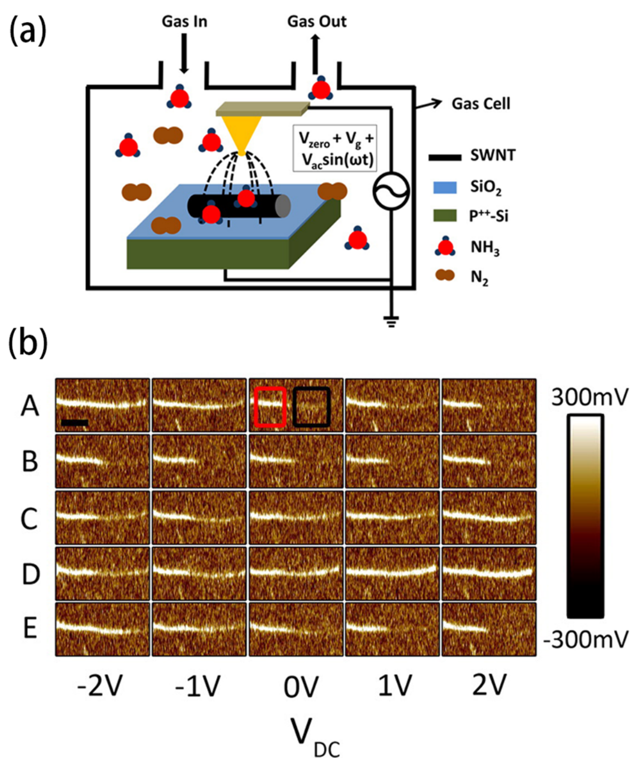

Figure 7. (a) Schematic illustration of DFM experiment with gas environment control. (b) Dielectric response images of a SWNT with an M−S intratube junction in different concentrations of NH_3 and at varied local gate voltages. Reproduced from ref 42. Copyright 2012 American Chemical Society.

These results indicate that there is a charge transfer between NH_3 and the SWNT, in which the SWNT is electronically doped and thus the hole concentration in semiconducting SWNTs is significantly depleted upon exposure to NH_3. This is an intrinsic interaction between SWNTs and NH_3, without interference of metal contact to SWNTs. These results are consistent with previous observations about SWNT-based FETs interacting with NH_3 in either gaseous or aqueous phases[44−46] and clearly demonstrate the *in situ* measurement capability of the DFM technique.

■ GATE MODULATION RATIO IN DFM

A gate modulation ratio, defined as the ratio of the DFM signal at different gate voltages, for example, at V_g = 2 V to that at V_g = −2 V (S_{2V}/S_{-2V}), is found to be a facile parameter that indicates the electronic properties of nanomaterials.[19] This ratio is a measure of the degree to which the charge carrier density is modulated by the gate voltage. Gate modulation ratio (S_{2V}/S_{-2V}) values close to 1 indicate gate independent carrier density and thus imply metallic behavior, and gate modulation ratio values less than 1 indicate p-type semiconducting behavior (Figure 8). Gate modulation ratio (S_{2V}/S_{-2V}) values greater than 1 are expected for n-type semiconducting nanomaterials. Since the gate modulation ratio is taken directly from the original DFM signal strengths without converting it to the dielectric force, the tip calibration process can be waived. More importantly, since it is independent of tip and imaging conditions, the data measured by multiple tips with different tip apex geometries may be combined in one set without calibration or normalization, so the wearing of the tip is no longer a limiting factor for the DFM-based metallicity assay,

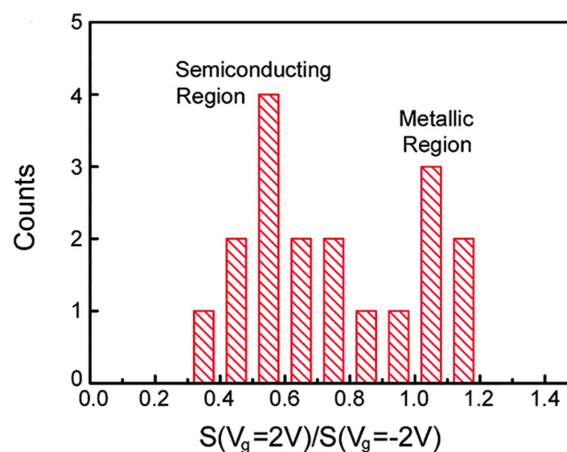

Figure 8. Histogram of gate modulation ratio of 18 SWNTs. Reproduced from ref 19. Copyright 2012 American Chemical Society.

DOI: 10.1021/acs.accounts.5b00046
Acc. Chem. Res. 2015, 48, 1788−1796

and a large number of SWNT samples can be measured to get reliable statistical results.[19]

QUANTITATIVE COMPARISON BETWEEN DFM AND FET MEASUREMENTS

The DFM gate modulation ratio discussed above not only is a convenient parameter for determining SWNT metallicity but also reflects true material properties in an astonishing way. Direct comparison between DFM and FET transport measurements on the same individual SWNTs reveals that the gate modulation ratio is linearly proportional to the logarithm of FET device on/off ratio.[24]

Figure 9 shows the DFM and FET characterization of the same exact SWNTs. The data in Figure 9a shows that the DFM

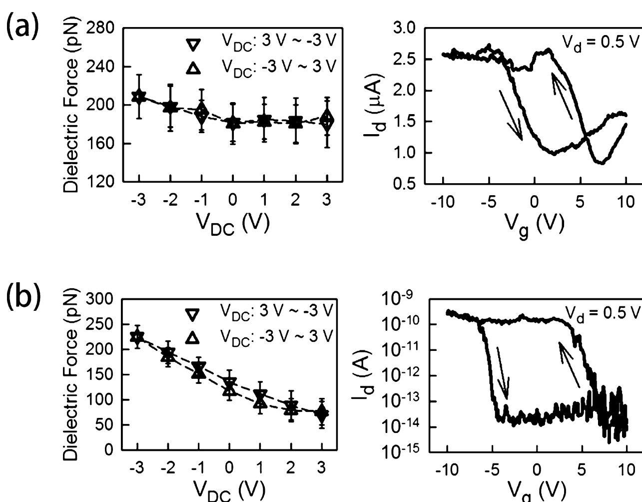

Figure 9. Dielectric force vs DC bias plots and transfer characteristics of a metallic (a) and a semiconducting (b) SWNT. A source−drain voltage of 0.5 V is used in the transfer characteristic measurements. Reproduced from ref 24, Copyright 2014. With kind permission from Springer Science and Business Media.

signal of this particular SWNT is essentially invariant under different gate bias, and the FET transport characteristics verify the metallic nature of this tube. In contrast, the SWNT in Figure 9b exhibits weak DFM signal at positive gate voltage and displays monotonically increasing DFM signal as the gate voltage decreases. This observation is consistent with previous characterization of p-type doped semiconducting SWNTs. The transconductance measurement on the corresponding device shows typical characteristics of p-type FET with $\sim10^4$ on/off ratio, again confirming the DFM determination of the tube's metallicity. It is noteworthy that both measurements exhibit hysteresis of the same direction as a result of charge trapping effect.[24,47,48] The apparent smaller hysteresis in DFM could be due to it only reflecting the properties of the channel material without the influence of the contacts.

Importantly, Figure 10 presents that the DFM gate modulation ratio is directly related with the FET device on/off ratio for the six semiconducting SWNTs we have measured. This direct correlation has far-reaching implications: first of all, it indicates that the dielectric response in the DFM experiment is a true measurement of transfer characteristics and parameters such as the gate modulation ratio reflect intrinsic material properties; second, from technological application point of view, the contactless DFM imaging technique is directly related

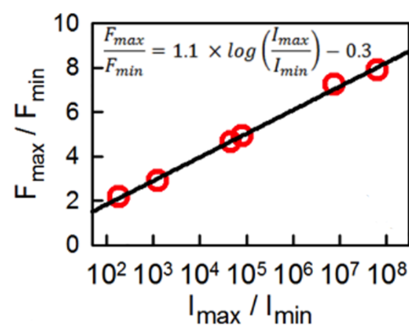

Figure 10. Gate modulation ratio of a tube in DFM against the on/off ratio of the same tube in FET for six semiconducting SWNTs. Symbols are experimental data, and solid line is the linear fitting. Reproduced from ref 24, Copyright 2014. With kind permission from Springer Science and Business Media.

to critical parameters in device applications and thus can be used to predict the device performance before the material is fabricated into devices. Furthermore, this correlation reveals the parallel between the DFM and FET characterization methods. The gate voltage in both experiments modulates the charge carrier density in the SWNT, and the experimental observables, the source−drain current in the FET case and the dielectric response in the DFM case, are both critically dependent on the carrier density and mobility. Such an underlying parallel forms the basis for the observed consistency between the DFM and the FET experiments on the same tubes. The major difference is that DFM is a contactless technique: the material under investigation is not electrically connected with an external circuit and thus there is no net carrier flow in or out of the material upon local gate modulation.

A Drude-level model is employed to understand the relation between the macroscopic DFM observable, that is, dielectric force, and the microscopic characteristics of the material, that is, charge carrier density ρ and mobility μ. As illustrated in Figure 11a, the DFM tip, which is represented with a point charge $q = CV$, is placed above the SWNT with distance d. The external field due to the charged DFM tip causes charge carriers to redistribute in the SWNT. The carrier (hole) density, $\rho(x,t)$, obeys the continuity equation:

$$\frac{\partial\rho(x,t)}{\partial t} + \mu\frac{\partial}{\partial x}\left[\rho(x,t)E_x - \frac{k_B T_0}{e}\frac{\partial\rho(x,t)}{\partial x}\right] = 0 \quad (2)$$

where E_x is the effective electric field along the nanotube, k_B is the Boltzmann constant, T_0 is the temperature, and e is the elementary charge. Figure 11b shows the numerically solved carrier density profiles in the SWNT at $t = 0$ and $3T/4$, where T is the period of the AC signal. The evolution of carrier density right beneath the tip from $t = 0$ to $t = T$ is shown in the inset. The total force experienced by the DFM tip is

$$F(t) = \frac{edC(V_{dc} + V_{ac}\sin(\omega t))}{4\pi\varepsilon_0}\int_{-L/2}^{L/2}\frac{\rho(x,t)}{(x^2 + d^2)^{3/2}} \quad (3)$$

where C is the capacitance and ε_0 is the vacuum permittivity. The DFM force can be obtained from the 2ω component of the Fourier transformation of eq 3. Figure 11c shows the numerically calculated dielectric force as a function of carrier density (black) and carrier mobility (red). The dependence of the dielectric force on the carrier mobility μ agrees well with physical intuition: when μ approaches zero, the carriers are essentially bounded at their equilibrium position and thus do

DOI: 10.1021/acs.accounts.5b00046
Acc. Chem. Res. 2015, 48, 1788−1796

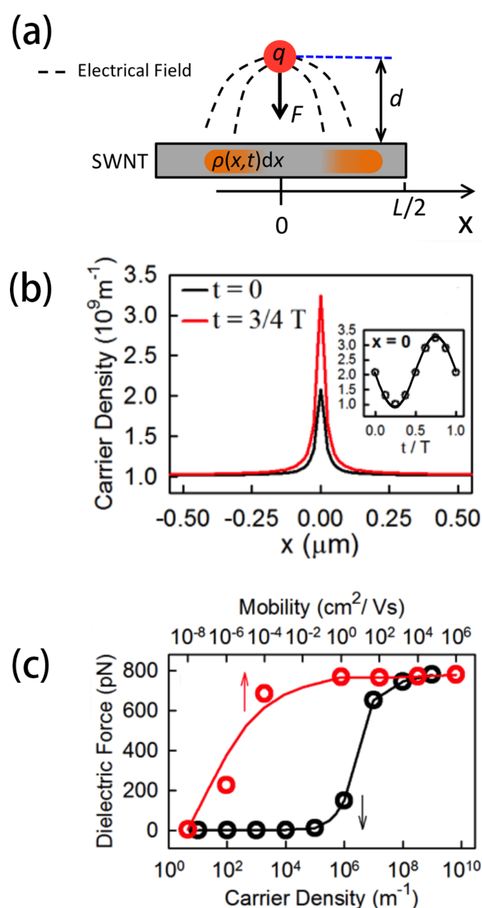

Figure 11. (a) The schematic illustration of the Drude-level model for DFM measurement, in which the orange-colored objects represent charge carriers in the nanotube. (b) Carrier density profiles along the SWNT at $t = 0$ (black) and $t = 3T/4$ (red). Inset shows the evolution of carrier density beneath the tip within one period of the AC bias. (c) Numerical simulation results of the dielectric force as a function of carrier density (black) and mobility (red). Symbols are the numerical data and lines are guide to eyes. The carrier density and mobility used in the numerical simulation are $\rho = 10^9$ m^{-1} (red) and $\mu = 10^6$ cm^2/(V s) (black). Reproduced from ref 24, Copyright 2014. With kind permission from Springer Science and Business Media.

not contribute to the dielectric response; for $\mu > 10^{-8}$ cm^2/(V s), the DFM force rapidly increases as μ increases and saturates at $\mu \approx 1$ cm^2/(V s). This saturation is due to the finite length of the nanotube, which has also been experimentally observed previously.[49] Because the dielectric force saturates at a fairly low mobility, the DFM signal is independent of μ for materials with high mobility such as SWNTs. The DFM force is sensitively dependent on the mean carrier density ρ_0 when $\rho_0 \gtrsim 10^5$ m^{-1}, which explains the tip voltage gating effect observed in DFM experiments. Within a certain range, the calculated dielectric force can be considered roughly correlated with the logarithm of the carrier density; since the source−drain current in FET transport is linearly proportional to carrier density, this also qualitatively explains the semilogarithmic correlation between DFM gate modulation ratio and FET device on/off ratio. More derivation and proof of the relationship are detailed in ref 21.

■ CONCLUSION AND OUTLOOK

DFM is a powerful tool in probing local electrical conductivity of nanomaterials without the need to make electrical contacts. The contactless imaging feature renders it well suited for characterization of heterogeneous samples. The spatial resolution and *in situ* measurement capability suggest widespread applications in mapping spatial variations in nanomaterials and correlating them with structural and morphological features of the system.

Future developments of the DFM technique may involve continuous improvements in signal sensitivity and spatial resolution, which will enable more applications in different materials systems such as two-dimensional graphene, transition metal dichalcogenides, and single crystalline metal sheets. Potential challenges lie in the establishment of continuum dielectric model or microscopic charge carrier model to extract quantitative properties of these materials. The intrinsic parallel between the DFM and FET measurements as outlined above may hint at the development of a technique directed toward quantification of local charge carrier concentration and mobility. The mapping of carrier concentration in an operating device would basically resolve the diffusion current in a device and would thus be greatly helpful in the understanding of device operation. Furthermore, probing of high frequency dielectric response and high frequency carrier properties is also an important direction to push provided that the resonance of the DFM tip/cantilever can be raised above the double of the interesting frequency.

■ AUTHOR INFORMATION

Corresponding Author

*E-mail: lwchen2008@sinano.ac.cn.

Present Addresses

‖Department of Chemistry, University of Washington, Seattle, WA 98195, USA.
⊥Department of Materials Science and Engineering, University of Wisconsin—Madison, Madison, WI 53706, USA.

Notes

The authors declare no competing financial interest.

Biographies

Jie Zhang is currently a postdoctoral research associate at University of Washington (Prof. D. S. Ginger). He received his B.S. and Ph.D. degrees from University of Science and Technology of China (USTC, Prof. X. Wang) in 2007 and 2013, respectively. He worked as a predoctoral research assistant at Suzhou Institute of Nano-tech and Nano-bionics (SINANO), Chinese Academy of Sciences (CAS), 2009−2013 (Prof. L. Chen). His current research interests are the dynamic properties of photoinduced charge carriers in solar cells and the dynamic melting properties of DNA.

Wei Lu is a professor at SINANO, CAS. He obtained his Ph.D. at USTC in 2005. He worked as a postdoctoral research fellow at Ohio University until 2008. He joined SINANO in 2008. His main research interests involve SPM and electrochemical energy storage.

Yize Stephanie Li completed her Ph.D. in 2009 at the University of Virginia. She carried out postdoctoral research at the University of Illinois at Urbana−Champaign and worked as a visiting scholar at SINANO. She joined the University of Wisconsin—Madison as a postdoctoral research associate in March 2013. Her current research interest is semiconductor-nanomembrane-based novel materials and devices.

Jinhua Cai received his B.Sc. and Ph.D. degrees in condensed matter physics from Nanjing University. He worked at the department of

DOI: 10.1021/acs.accounts.5b00046
Acc. Chem. Res. 2015, 48, 1788−1796

physics, Shanghai Jiao Tong University, from 1999 to 2013 as a postdoctoral researcher and an associate professor. He is currently an associate professor at SINANO. His current research focuses on photovoltaic material and device physics.

Liwei Chen is a Professor of Physical Chemistry at SINANO. He received his B. S. from USTC, M.S. from Peking University, and Ph.D. in Chemistry from Harvard University (Prof. C. M. Lieber). He then worked as postdoctoral research fellow at Columbia University (Prof. L. E. Brus) and taught at Ohio University as an assistant professor from 2004 through 2008. He joined SINANO in 2009. His current research program focuses on the materials and interfaces in energy nanotechnology.

■ ACKNOWLEDGMENTS

The authors thank collaborators throughout this long-term project, whose names are specified in relevant original papers. We acknowledge financial support at different stages of this program from National Natural Science Foundation of China (Grant Nos. 21473242, 91233104, 20973122, 61376063, and 21273273), Strategic Priority Research Program of the Chinese Academy of Sciences (Grant No. XDA09010600), American Chemical Society Petroleum Research Fund, and the Collaborative Innovation Center of Suzhou Nano Science and Technology. L.W.C. also thanks the Natural Science Foundation of Jiangsu Province (Grant BK20130006) for support.

■ REFERENCES

(1) Dai, H. J. Carbon Nanotubes: Synthesis, Integration, and Properties. *Acc. Chem. Res.* **2002**, *35*, 1035−1044.
(2) Avouris, P. Molecular Electronics with Carbon Nanotubes. *Acc. Chem. Res.* **2002**, *35*, 1026−1034.
(3) Wu, J. S.; Pisula, W.; Mullen, K. Graphenes as Potential Material for Electronics. *Chem. Rev.* **2007**, *107*, 718−747.
(4) Wang, Q. H.; Kalantar-Zadeh, K.; Kis, A.; Coleman, J. N.; Strano, M. S. Electronics and Optoelectronics of Two-Dimensional Transition Metal Dichalcogenides. *Nat. Nanotechnol.* **2012**, *7*, 699−712.
(5) Ebbesen, T. W.; Lezec, H. J.; Hiura, H.; Bennett, J. W.; Ghaemi, H. F.; Thio, T. Electrical Conductivity of Individual Carbon Nanotubes. *Nature* **1996**, *382*, 54−56.
(6) Tans, S. J.; Verschueren, A. R. M.; Dekker, C. Room-Temperature Transistor Based on a Single Carbon Nanotube. *Nature* **1998**, *393*, 49−52.
(7) Novoselov, K. S.; Geim, A. K.; Morozov, S. V.; Jiang, D.; Zhang, Y.; Dubonos, S. V.; Grigorieva, I. V.; Firsov, A. A. Electric Field Effect in Atomically Thin Carbon Films. *Science* **2004**, *306*, 666−669.
(8) Cui, Y.; Duan, X. F.; Hu, J. T.; Lieber, C. M. Doping and Electrical Transport in Silicon Nanowires. *J. Phys. Chem. B* **2000**, *104*, 5213−5216.
(9) Ilani, S.; Donev, L. A. K.; Kindermann, M.; McEuen, P. L. Measurement of the Quantum Capacitance of Interacting Electrons in Carbon Nanotubes. *Nat. Phys.* **2006**, *2*, 687−691.
(10) Zhang, Y. B.; Tan, Y. W.; Stormer, H. L.; Kim, P. Experimental Observation of the Quantum Hall Effect and Berry's Phase in Graphene. *Nature* **2005**, *438*, 201−204.
(11) Mueller, T.; Xia, F.; Avouris, P. Graphene Photodetectors for High-Speed Optical Communications. *Nat. Photonics* **2010**, *4*, 297−301.
(12) Sze, S. M.; Ng, K. K. *Physics of Semiconductor Devices*, 3rd ed.; John Wiley & Sons, Inc.: Hoboken, NJ, 2006.
(13) Pierret, R. F. *Field Effect Devices*; Addison-Wesley Publishing Company Inc.: Reading, MA, 1990.
(14) Williams, C. C. Two-Dimensional Dopant Profiling by Scanning Capacitance Microscopy. *Annu. Rev. Mater. Sci.* **1999**, *29*, 471−504.
(15) Lai, K.; Peng, H.; Kundhikanjana, W.; Schoen, D. T.; Xie, C.; Meister, S.; Cui, Y.; Kelly, M. A.; Shen, Z.-X. Nanoscale Electronic Inhomogeneity in In2se3 Nanoribbons Revealed by Microwave Impedance Microscopy. *Nano Lett.* **2009**, *9*, 1265−1269.
(16) Martin, Y.; Abraham, D. W.; Wickramasinghe, H. K. High-Resolution Capacitance Measurement and Potentiometry by Force Microscopy. *Appl. Phys. Lett.* **1988**, *52*, 1103−1105.
(17) Hoepker, N.; Lekkala, S.; Loring, R. F.; Marohn, J. A. Dielectric Fluctuations over Polymer Films Detected Using an Atomic Force Microscope. *J. Phys. Chem. B* **2011**, *115*, 14493−14500.
(18) Russell, E. V.; Israeloff, N. E.; Walther, L. E.; Alvarez Gomariz, H. Nanometer Scale Dielectric Fluctuations at the Glass Transition. *Phys. Rev. Lett.* **1998**, *81*, 1461−1464.
(19) Lu, W.; Zhang, J.; Li, Y. S.; Chen, Q.; Wang, X. P.; Hassanien, A.; Chen, L. W. Contactless Characterization of Electronic Properties of Nanomaterials Using Dielectric Force Microscopy. *J. Phys. Chem. C* **2012**, *116*, 7158−7163.
(20) Lu, W.; Wang, D.; Chen, L. W. Near-Static Dielectric Polarization of Individual Carbon Nanotubes. *Nano Lett.* **2007**, *7*, 2729−2733.
(21) Girard, P. Electrostatic Force Microscopy: Principles and Some Applications to Semiconductors. *Nanotechnology* **2001**, *12*, 485.
(22) Cherniavskaya, O.; Chen, L. W.; Weng, V.; Yuditsky, L.; Brus, L. E. Quantitative Noncontact Electrostatic Force Imaging of Nanocrystal Polarizability. *J. Phys. Chem. B* **2003**, *107*, 1525−1531.
(23) Lu, W.; Xiong, Y.; Hassanien, A.; Zhao, W.; Zheng, M.; Chen, L. W. A Scanning Probe Microscopy Based Assay for Single-Walled Carbon Nanotube Metallicity. *Nano Lett.* **2009**, *9*, 1668−1672.
(24) Li, Y.; Ge, J.; Cai, J.; Zhang, J.; Lu, W.; Liu, J.; Chen, L. Contactless Probing of the Intrinsic Carrier Transport in Single-Walled Carbon Nanotubes. *Nano Res.* **2014**, *7*, 1623−1630.
(25) Benedict, L. X.; Louie, S. G.; Cohen, M. L. Static Polarizabilities of Single-Wall Carbon Nanotubes. *Phys. Rev. B* **1995**, *52*, 8541−8549.
(26) Jensen, L.; Schmidt, O. H.; Mikkelsen, K. V.; Åstrand, P.-O. Static and Frequency-Dependent Polarizability Tensors for Carbon Nanotubes. *J. Phys. Chem. B* **2000**, *104*, 10462−10466.
(27) Novikov, D. S.; Levitov, L. S. Energy Anomaly and Polarizability of Carbon Nanotubes. *Phys. Rev. Lett.* **2006**, *96*, No. 036402.
(28) Kozinsky, B.; Marzari, N. Static Dielectric Properties of Carbon Nanotubes from First Principles. *Phys. Rev. Lett.* **2006**, *96*, No. 166801.
(29) Krupke, R.; Hennrich, F.; Löhneysen, H. v.; Kappes, M. M. Separation of Metallic from Semiconducting Single-Walled Carbon Nanotubes. *Science* **2003**, *301*, 344−347.
(30) Krupke, R.; Hennrich, F.; Weber, H. B.; Kappes, M. M.; v. Löhneysen, H. Simultaneous Deposition of Metallic Bundles of Single-Walled Carbon Nanotubes Using Ac-Dielectrophoresis. *Nano Lett.* **2003**, *3*, 1019−1023.
(31) Peng, H.; Alvarez, N. T.; Kittrell, C.; Hauge, R. H.; Schmidt, H. K. Dielectrophoresis Field Flow Fractionation of Single-Walled Carbon Nanotubes. *J. Am. Chem. Soc.* **2006**, *128*, 8396−8397.
(32) Zeng, H.; Zhao, H.; Zhang, F.-C.; Cui, X. Observation of Exciton-Phonon Sideband in Individual Metallic Single-Walled Carbon Nanotubes. *Phys. Rev. Lett.* **2009**, *102*, No. 136406.
(33) Revilla, R. I.; Li, X.-J.; Yang, Y.-L.; Wang, C. Comparative Method to Quantify Dielectric Constant at Nanoscale Using Atomic Force Microscopy. *J. Phys. Chem. C* **2014**, *118*, 5556−5562.
(34) Fumagalli, L.; Ferrari, G.; Sampietro, M.; Gomila, G. Dielectric-Constant Measurement of Thin Insulating Films at Low Frequency by Nanoscale Capacitance Microscopy. *Appl. Phys. Lett.* **2007**, *91*, No. 243110.
(35) Fumagalli, L.; Ferrari, G.; Sampietro, M.; Gomila, G. Quantitative Nanoscale Dielectric Microscopy of Single-Layer Supported Biomembranes. *Nano Lett.* **2009**, *9*, 1604−1608.
(36) Fumagalli, L.; Esteban-Ferrer, D.; Cuervo, A.; Carrascosa, J. L.; Gomila, G. Label-Free Identification of Single Dielectric Nanoparticles and Viruses with Ultraweak Polarization Forces. *Nat. Mater.* **2012**, *11*, 808−816.
(37) Jiang, Y. P.; Qi, Q.; Wang, R.; Zhang, J.; Xue, Q. K.; Wang, C.; Jiang, C.; Qiu, X. H. Direct Observation and Measurement of Mobile

DOI: 10.1021/acs.accounts.5b00046
Acc. Chem. Res. 2015, 48, 1788−1796

Charge Carriers in a Monolayer Organic Semiconductor on a Dielectric Substrate. *ACS Nano* **2011**, *5*, 6195−6201.

(38) Li, J.; He, Y. J.; Han, Y. M.; Liu, K.; Wang, J. P.; Li, Q. Q.; Fan, S. S.; Jiang, K. L. Direct Identification of Metallic and Semiconducting Single-Walled Carbon Nanotubes in Scanning Electron Microscopy. *Nano Lett.* **2012**, *12*, 4095−4101.

(39) Kang, D.; Park, N.; Ko, J. H.; Bae, E.; Park, W. Oxygen-Induced P-Type Doping of a Long Individual Single-Walled Carbon Nanotube. *Nanotechnology* **2005**, *16*, 1048−1052.

(40) Shim, M.; Back, J. H.; Ozel, T.; Kwon, K. W. Effects of Oxygen on the Electron Transport Properties of Carbon Nanotubes: Ultraviolet Desorption and Thermally Induced Processes. *Phys. Rev. B* **2005**, *71*, No. 205411.

(41) Goldberger, J.; Sirbuly, D. J.; Law, M.; Yang, P. ZnO Nanowire Transistors. *J. Phys. Chem. B* **2004**, *109*, 9−14.

(42) Zhang, J.; Lu, W.; Li, Y. S.; Lu, D.; Zhang, T.; Wang, X. P.; Chen, L. W. Probing Electronic Doping of Single-Walled Carbon Nanotubes by Gaseous Ammonia with Dielectric Force Microscopy. *J. Phys. Chem. Lett.* **2012**, *3*, 3509−3512.

(43) Cui, X. D.; Freitag, M.; Martel, R.; Brus, L.; Avouris, P. Controlling Energy-Level Alignments at Carbon Nanotube/Au Contacts. *Nano Lett.* **2003**, *3*, 783−787.

(44) Kong, J.; Franklin, N. R.; Zhou, C. W.; Chapline, M. G.; Peng, S.; Cho, K. J.; Dai, H. J. Nanotube Molecular Wires as Chemical Sensors. *Science* **2000**, *287*, 622−625.

(45) Bradley, K.; Gabriel, J. C. P.; Briman, M.; Star, A.; Gruner, G. Charge Transfer from Ammonia Physisorbed on Nanotubes. *Phys. Rev. Lett.* **2003**, *91*, No. 218301.

(46) Peng, N.; Zhang, Q.; Chow, C. L.; Tan, O. K.; Marzari, N. Sensing Mechanisms for Carbon Nanotube Based NH_3 Gas Detection. *Nano Lett.* **2009**, *9*, 1626−1630.

(47) Kim, W.; Javey, A.; Vermesh, O.; Wang, Q.; Li, Y.; Dai, H. Hysteresis Caused by Water Molecules in Carbon Nanotube Field-Effect Transistors. *Nano Lett.* **2003**, *3*, 193−198.

(48) Lee, J. S.; Ryu, S.; Yoo, K.; Choi, I. S.; Yun, W. S.; Kim, J. Origin of Gate Hysteresis in Carbon Nanotube Field-Effect Transistors. *J. Phys. Chem. C* **2007**, *111*, 12504−12507.

(49) Lu, W.; Xiong, Y.; Chen, L. W. Length-Dependent Dielectric Polarization in Metallic Single-Walled Carbon Nanotubes. *J. Phys. Chem. C* **2009**, *113*, 10337−10340.

DOI: 10.1021/acs.accounts.5b00046
Acc. Chem. Res. 2015, 48, 1788−1796